Letter

Essential role of magnetic frustration in the phase diagrams of doped cobaltites

Peter P. Orth,[1,2,*] D. Phelan,[3,4] J. Zhao,[3] H. Zheng,[3] J. F. Mitchell,[3] C. Leighton,[4] and Rafael M. Fernandes[5]

[1]*Ames Laboratory, Ames, Iowa 50011, USA*

[2]*Department of Physics and Astronomy, Iowa State University, Ames, Iowa 50011, USA*

[3]*Materials Science Division, Argonne National Laboratory, Lemont, Illinois 60439, USA*

[4]*Department of Chemical Engineering and Materials Science, University of Minnesota, Minneapolis, Minnesota 55455, USA*

[5]*School of Physics and Astronomy, University of Minnesota, Minneapolis, Minnesota 55455, USA*

(Received 18 May 2021; revised 25 October 2021; accepted 14 June 2022; published 5 July 2022)

Doped perovskite cobaltites (e.g., $La_{1-x}Sr_xCoO_3$) have been extensively studied for their spin-state physics, electronic inhomogeneity, and insulator-metal transitions. Ferromagnetically interacting spin-state polarons emerge at low x in the phase diagram of these compounds, eventually yielding long-range ferromagnetism. The onset of long-range ferromagnetism ($x \approx 0.18$) is substantially delayed relative to polaron percolation ($x \approx 0.05$), however, generating a troubling inconsistency. Here, Monte Carlo simulations of a disordered classical spin model are used to establish that previously ignored *magnetic frustration* is responsible for this effect, enabling faithful reproduction of the magnetic phase diagram.

DOI: 10.1103/PhysRevMaterials.6.L071402

Introduction and experimental situation. The insulator-metal transition (IMT) is an important, widely observed phenomenon in condensed matter physics that continues to be intensively studied [1]. While there are various mechanisms by which IMTs occur, in quantum materials, the percolation of conductive regions in an insulating matrix, driven by temperature, doping, pressure, etc., is widespread [1–5]. The microscopic factors inducing such electronic inhomogeneity (across nano- to mesoscales) include structural disorder, multiple competing interactions, and coupled degrees of freedom, resulting in a formidable problem [1,6,7].

Doped perovskite cobaltites, with $La_{1-x}Sr_xCoO_3$ (LSCO) as the archetype, have proven to be paradigmatic for investigations of such percolative IMTs [8–12]. Experimental studies of LSCO single crystals culminate in the electronic/magnetic phase diagram in Fig. 1, which we have constructed from both published and new data (see Supplemental Material Sec. S1 [13]). At $x = 0$ [undoped $LaCoO_3$ (LCO)], the Co^{3+} (d^6) ions adopt an $S = 0$ diamagnetic insulating ground state, but with a spin gap of only ~10 meV due to comparable crystal field and Hund's exchange energies, leading to the famous thermally excited spin-state transition (SST) [9–12,14–18]. Defined as the midpoint of the resulting rise in susceptibility, the SST occurs at $T_{SST} \approx 70$ K (Fig. 1). It is essentially complete by approximately 120 K, above which antiferromagnetic (AF) Co^{3+}-Co^{3+} superexchange interactions occur, resulting in the negative Curie-Weiss temperature (θ_{CW}) [19–21] shown in Fig. 1.

Fascinating behavior emerges upon dilute hole doping (e.g., $x = 0.005$), where giant magnetic moments ($S \approx 13/2$) occur due to seven-site, octahedrally shaped spin-state polarons (Fig. 2, inset) [21,27–29]. In essence, doped Co^{4+} ions stabilize finite spin states on neighboring Co^{3+} ions, forming a spin-state polaron with ferromagnetic (F) intrapolaron interactions. As noted previously, and borne out by our own data (Fig. 2, right axis), increasing x leads to polaron overlap [27], and thus collapse of the magnetization per hole [21]. As shown in Fig. 1, this is accompanied by a rapid increase in θ_{CW} (decrease in $|\theta_{CW}|$), which inverts from negative to positive [19,21] at $x \approx 0.04$, reflecting the dominance of intrapolaron F Co^{4+}-Co^{3+} interactions over extrapolaron AF Co^{3+}-Co^{3+} interactions. At this pivotal $x \approx 0.04$ (vertical dashed line, Fig. 1) multiple experimental probes indicate short-range F order, including small-angle neutron scattering (SANS) [10], inelastic neutron spectroscopy [21], neutron diffraction [12,30], and specific heat [10,22]. As shown in the phase diagram, signatures of nanoscale magnetic inhomogeneity then turn on at temperature T^*, followed at a lower T_G by spin/cluster-glass freezing. Most dramatically, a percolation transition then occurs at $x_c \approx 0.18$ (solid vertical line, Fig. 1), where a low-temperature IMT occurs and long-range F order is detected by neutron diffraction [12,31], SANS [10,11], and magnetometry [8,9]. In Fig. 2 this is reflected in a sharp upturn in magnetization (blue, right axis) and F volume fraction (black, right axis). This percolation transition can also be controlled with voltage in electrolyte-gated LSCO [32,33]. A final important composition on the phase diagram is at $x \approx 0.22$ (vertical line, Fig. 1), where multiple probes (e.g., SANS, specific heat, La NMR, magnetotransport [10,24]) reveal *uniform* long-range F order, i.e., an end to the low T magnetically phase-separated regime [10]. T_C gradually increases with further doping, reaching 250 K at $x = 0.5$.

The picture that emerges from the above, i.e., spin-state polarons generating nanoscale F regions that percolate into long-range F order at $x_c \approx 0.18$, has become widely accepted. This masks a troubling inconsistency, however. Specifically, simple statistical arguments indicate that a percolation of seven-site polarons into a long-range F network should

*porth@iastate.edu

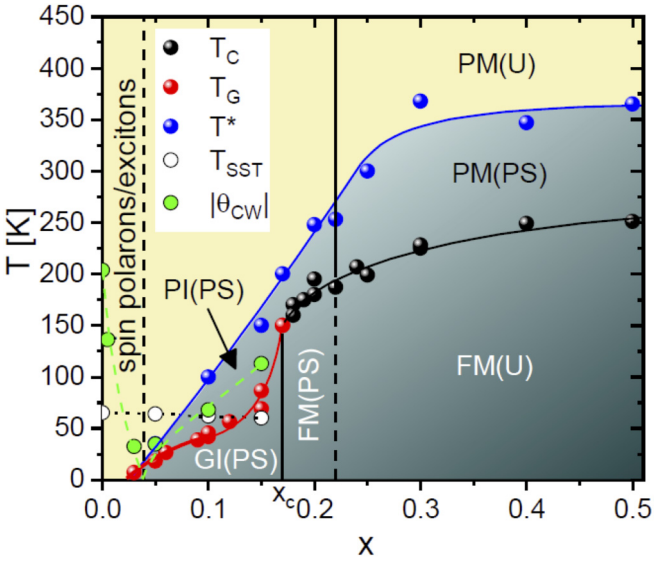

FIG. 1. Magnetic/electronic phase diagram of single-crystal $La_{1-x}Sr_xCoO_3$ (LSCO). Shown are the Curie temperature (T_C), spin/cluster glass freezing temperature (T_G), onset temperature for ferromagnetic (F) fluctuations/clusters (T^*), and non-F matrix spin-state crossover temperature (T_{SST}). Superimposed is the magnitude of the Curie-Weiss temperature θ_{CW}, which inverts from antiferromagnetic (AF) to F at $x \approx 0.04$. FM = ferromagnetic metal, PM = paramagnetic metal, PI = paramagnetic insulator, and GI = glassy magnetic insulator; U designates uniform states, and PS magnetically/electronically phase separated states. T_C, T_G, T^*, and θ_{CW} are from this Letter, supplemented with Refs. [10,22–24]; T_{SST} data are taken from Ref. [25]. The vertical line at $x_c = 0.18$ marks the cluster percolation threshold, and the vertical line at $x = 0.22$ the transition from PS to U states at low temperature (and from negative to positive temperature coefficient of resistance at high temperature). For $x > 0.30$, where single-crystal data are not available, T_C and T^* values from polycrystalline samples have been used [26].

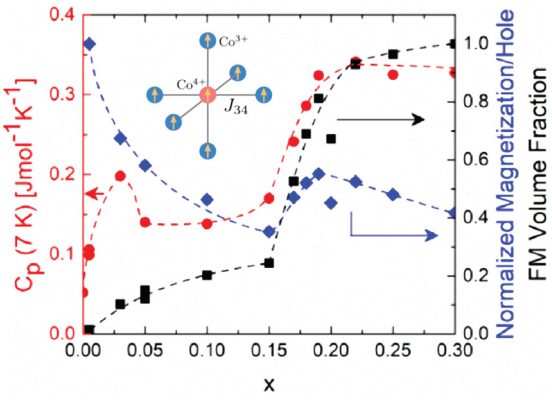

FIG. 2. Doping (x) dependence of the 7-K heat capacity (C_p, red, left axis), magnetization per hole (blue, right axis, normalized to the $x = 0$ value), and F volume fraction (black, right axis). The latter is estimated by extrapolating the high-field magnetization-field behavior to zero field. Dashed lines are guides to the eye. Inset: Schematic of seven-site spin-state polaron with F exchange coupling J_{34} between sites.

occur at $x \approx 0.04$. This can be understood by dividing the cubic (LSCO is cubic above $x \approx 0.5$ and mildly rhombohedrally distorted at lower x) site percolation threshold of $s_c = 0.31$ by 7 (the number of sites in the polaron), yielding $x = s_c/7 = 0.044$. The number of *isolated* polarons in fact peaks at $x \approx 0.03$ [see Fig. 3(b), inset], prior to percolation of the polarons at $x \approx 0.04$. As discussed in the Supplemental Material, Sec. S2 [13], the low-T specific heat C_p (e.g., at 7 K, left axis, Fig. 2) supports this, with the Schottky specific-heat signature of the spin-state polarons peaking at $x = 0.03$ then leveling off at $x = 0.05$, before rising again at $x > x_c$ due to electronic contributions to C_p in the F metallic state [10,22]. Critically, this doping level at which polaron percolation is expected ($x \approx 0.04$) is substantially lower than the experimentally observed $x_c \approx 0.18$ at which percolation to a long-range F metallic state occurs. In this Letter, we finally resolve this issue, using a model of interacting dilute and disordered magnetic moments that we investigate using large-scale Monte Carlo simulations. This reveals a vital role for *magnetic frustration*, a previously ignored factor in the phase diagrams of such materials. We expect this physics to also play a role in the phase behavior of other heavily studied doped cobaltites, such as $La_{1-x}Ca_xCoO_3$, $La_{1-x}Ba_xCoO_3$, $Pr_{1-x}Ca_xCoO_3$, etc. Moreover, while the spin-state aspect to the polarons is specific to cobaltites, frustration may also play a role in other systems exhibiting magnetic polaron to long-range order transitions, such as manganites.

Theoretical model. To address the question of what delays the onset of percolation in LSCO, we study an effective disordered Ising spin model that captures the essential microscopic physics. Starting from an empty cubic lattice, we randomly populate a fraction x of the sites with Ising spins $S_i^{(4)} = \pm 1$, corresponding to Co^{4+} ions. Two neighboring $S^{(4)}$ spins interact ferromagnetically with coupling constant $J_{44} < 0$, reflecting the fact that the Curie-Weiss temperature θ_{CW} is positive for $x \geqslant 0.05$ and the fully doped end member $SrCoO_3$ is F ($T_C \approx 300$ K). Note that we consider Ising spins here to account for the easy-axis anisotropy in the material. We then place spins $S_i^{(3)} = \pm 1$ on all empty sites neighboring an $S^{(4)}$ spin, which models the emergence of spin-state polarons due to transitions from LS (low-spin) to IS (intermediate-spin) states on the Co^{3+} sites neighboring a Co^{4+}. The nearest-neighbor interaction between $S_i^{(4)}$ and $S_j^{(3)}$ spins is also F, $J_{34} < 0$, leading to the formation of large spin S polaronic clusters, consisting of seven sites for an isolated polaron. In contrast, the interaction between two neighboring $S^{(3)}$ spins is AF, $J_{33} > 0$. This is consistent with a negative θ_{CW} for thermally excited IS Co^{3+} spins at $x < 0.05$. Note that as an Ising spin model, our model does not explicitly account for a change in itinerancy across the insulator-metal transition and onset of long-range F at $x = 0.18$. We argue that explicitly accounting for such itinerancy is not essential, as the essence of this transition is percolation of preexisting hole-rich F clusters, i.e., the ferromagnetism is in some sense itinerant on both sides of the transition. The fundamental change in character at this transition is thus from short- to long-range F, which our model captures, as shown below.

The presence of both F and AF interactions leads to frustration of polarons as shown in Fig. 3(a) for two neighboring polarons. In the F configuration shown, the F bonds J_{34} and J_{44} are satisfied, thus frustrating the AF bonds J_{33}. The fact

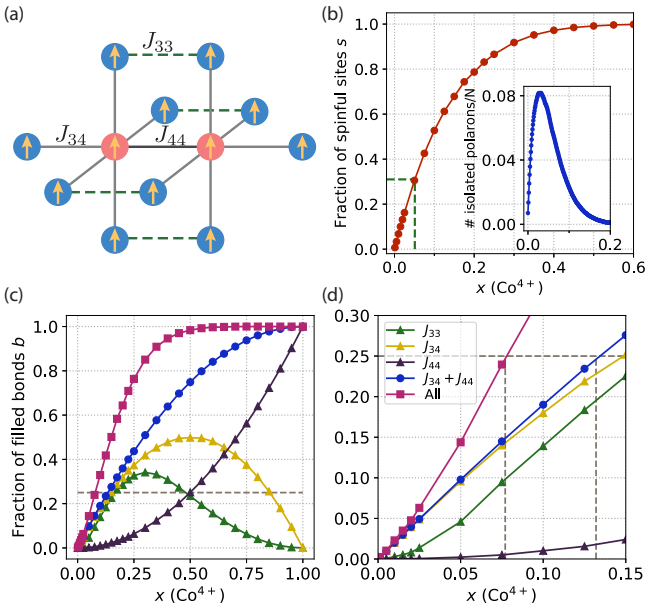

FIG. 3. (a) Schematic of two nearby seven-site polarons with exchange interactions $J_{34}, J_{44} < 0$ (F) and $J_{33} > 0$ (AF). Co^{4+} (Co^{3+}) sites are shown in red (blue). In this F configuration, the AF J_{33} bonds (green dashed) are frustrated. (b) Fraction of spinful sites s (either Co^{4+} or Co^{3+}) as a function of Co^{4+} doping x. The horizontal green dashed line denotes the site percolation threshold on the cubic lattice, $s_c = 0.31$, which is reached at $x = 0.05$. The inset shows the fraction of spins in isolated seven-site polarons, which peaks at $x = 0.03$. Data was obtained for system size $N = L^3$ with $L = 32$ and averaged over $N_{\rm dis} = 50$ disorder realizations. Inset data was obtained for system size $N = 10^3$ and is averaged over 10^3 disorder realizations. (c), (d) Fraction of filled bonds b as a function of Co^{4+} doping x. Different bonds are described in the legend; "All" refers to counting J_{33}, J_{34}, and J_{44} bonds. The horizontal gray line denotes the bond percolation threshold on the cubic lattice $b_c = 0.25$. The system exhibits only finite-size clusters for $x < 0.08$ ($b_{\rm All} < b_c$). If AF bonds were absent, the $T = 0$ paramagnetic-to-ferromagnetic transition would occur at $x = 0.13$ ($b_{(34)+(44)} = b_c$), when a macroscopic percolating cluster that only contains F J_{34} and J_{44} bonds emerges. However, the presence of AF J_{33} bonds decouples the percolation of F bonds from the onset of F order. Fraction of filled bonds was obtained for same parameters as filled sites in panel (b).

that the number of spinful sites s rapidly grows with the fraction x of Co^{4+} sites is shown in Fig. 3(b). Since an isolated polaron contains seven sites, the initial slope of the curve is $s \approx 7x$, which levels off once the polarons overlap at larger x. The maximal number of isolated polarons occurs at $x = 0.03$ [Fig. 3(b), inset]. This marks the onset of frustration, which suppresses the development of F order once a macroscopic site cluster forms at $x = 0.05$, where s reaches the site percolation threshold $s_c = 0.31$. Note that we neglect the weak correlation between the occupation probability of spinful sites as they are added as few-site polaronic clusters, which will result in a slightly larger numerical value of s_c. To further elucidate frustration, we investigate the phenomenological model Hamiltonian

$$H = J_{44} \sum_{\langle i,j\rangle_{44}} S_i^{(4)} S_j^{(4)} + J_{33} \sum_{\langle i,j\rangle_{33}} S_i^{(3)} S_j^{(3)} + J_{34} \sum_{\langle i,j\rangle_{34}} S_i^{(3)} S_j^{(4)}. \tag{1}$$

Here, $J_{44}, J_{34} < 0$ correspond to F and $J_{33} > 0$ to AF interactions and $\langle i, j\rangle_{ab}$ runs over all nearest-neighbor spinful sites of type a, b on the cubic lattice.

Let us first consider the limit $J_{33} = 0$, where only F interactions are present. As shown in Figs. 3(c) and 3(d), counting only J_{34} and J_{44} bonds (blue points), the bond percolation limit at $b_c = 0.25$ [34,35] is reached at Co^{4+} doping level $x_c^{(34)+(44)} = 0.13$ [Fig. 3(d) is a magnified view of Fig. 3(c) to enable this to be seen more clearly]. Since all interactions in this limit are F, this implies the emergence of a macroscopic F cluster (consisting solely of F bonds) and the onset of F order at $T = 0$. In contrast, considering $J_{33} \neq 0$ and counting *all* bonds (magenta points), a macroscopic percolating cluster emerges already at $x_c^{(33)+(34)+(44)} = 0.075$. Critically, however, $J_{33} > 0$ is AF, so the development of F order does *not* coincide with bond percolation. Instead, spins in the macroscopic cluster will experience frustration due to the random distribution of F and AF bonds, and we expect a spin-glass (SG) phase at low temperatures. This frustration is fully captured by an Ising interaction, justifying our neglect of quantum fluctuations. The degree of frustration is controlled by the ratios J_{33}/J_{34} and J_{33}/J_{44}, which also set the end point of the SG phase and the emergence of F order at larger x, as we show next.

We numerically investigate the model in Eq. (1) using large-scale parallel tempering Monte Carlo (MC) simulations. We simulate systems of size $N = L^3$ with $L = 8$, 12, 16 and for $N_{\rm dis} = 50$ (30) disorder realizations for $L = 8$ ($L = 12$, 16) using a combination of Metropolis and parallel-tempering updating steps. The total number of MC steps is $N_{\rm MC} = 8\times10^4$, 4×10^4, and 8×10^3 for increasing system sizes. We use the first half of these steps for thermalization and measure observables only during the second half of the simulation. Error bars are obtained using the standard jackknife method [36]. To connect to experiment, we choose the F exchange couplings to be equal $J_{34} = J_{44} = -1$, since the F transition temperature of LSCO varies only slightly from ~250 to ~300 K over the doping range $0.5 < x < 1$, whereas the bond number ratio b_{34}/b_{44} varies from two to zero over the same range [see Fig. 3(c)]. Because there are only few J_{44} bonds for small doping and $b_{44} < 0.06$ for $x < 0.25$, our results in this (insulating) range depend only weakly on J_{44}, justifying our choice of doping-independent values for J_{34} and J_{44}. Finally, we set $J_{33} = 0.2$, which corresponds to moderate frustration and gives $x_c = 0.25$, close to the experimentally observed value in LSCO. Results for other values of J_{33} are presented in the Supplemental Material, Secs. S4 and S5 [13]). A smaller value of J_{33} merely shifts x_c closer to $x = 0.13$, whereas a larger J_{34} results in an intermediate AF phase; this is in fact observed in some doped cobaltites, e.g., $La_{1-x}Ba_xCoO_3$ [37].

The resulting finite-temperature phase diagram as a function of x, and for $J_{34} = J_{44} = -1$, $J_{33} = 0.2$, is shown in Fig. 4(a); this is plotted over the same range of x shown in the phase diagram in Fig. 1. At large x, where F bonds dominate, the system enters a F phase at a transition temperature $T_{\rm F}(x)$ that is slightly smaller than the value $T_{\rm Ising}^{\rm 3D} = 4.5J_{44}$ of the $x = 1$ system due to missing bonds and AF J_{33} bonds in the macroscopic spin cluster. We obtain $T_{\rm F}$ from the crossing of the F Binder cumulants [38,39] $U_{\rm F} = \frac{3}{2}(1 - \frac{1}{3}\frac{[\langle m^4\rangle]_{\rm dis}}{[\langle m^2\rangle]_{\rm dis}^2})$ for different system sizes (see Supplemental Material Sec. S3).

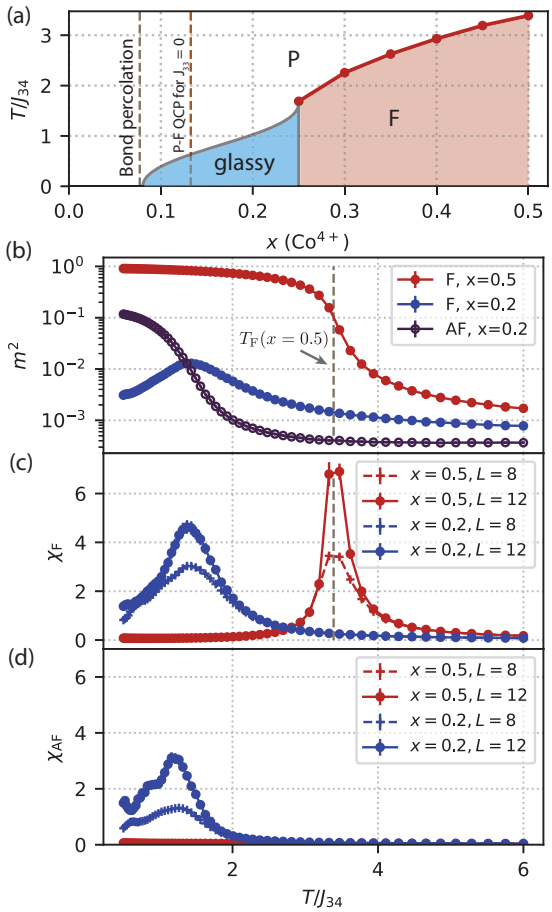

FIG. 4. (a) Numerical finite-temperature phase diagram of the frustrated J_{33}-J_{34}-J_{44} model as a function of Co^{4+} doping, obtained from percolation analysis and MC simulations. The different phases are paramagnetic (P), ferromagnetic (F), and glassy, which is characterized by short-range AF and F correlations. Couplings are set to $J_{34} = J_{44} = -1$ (F) and $J_{33} = 0.2$ (AF). Transition temperatures T_F (red dots) are obtained from MC simulations via crossing of F Binder cumulants (see Supplemental Material Sec. S3). Such crossings are notably absent for $x \leqslant 0.225$. The gray dashed line at $x = 0.08$ denotes the bond percolation threshold [$b_{All} = b_c$, see Fig. 3(d)]. The brown line denotes the $T = 0$ P-F quantum critical point (QCP) in the unfrustrated model ($J_{33} = 0$), obtained from $b_{(34)+(44)} = b_c$ in Fig. 3(d). The transition temperature to the glassy phase (solid gray line) is schematic and smoothly connects the various numerically obtained points. (b)–(d) MC simulation results of observables m_F^2, m_{AF}^2, χ_F, χ_{AF} for $x = 0.2$ and $x = 0.5$ and different system sizes, $L = 8, 12$. Long-range F order develops for $x = 0.5$, while only short-range F and AF correlations coexist at $x = 0.2$, which is characteristic of a glassy phase.

Here, $m = \frac{1}{N}\sum_{i=1}^{N} S_i$ is the magnetization, S_i is the spin at site i, and the brackets $\langle O\rangle$ ($[O]_{dis}$) denote thermal (disorder) averages.

$T_F(x)$ decreases as x is reduced and for $x \leqslant 0.225$ the crossing of the Binder cumulants is absent, implying that true long-range F order ceases to exist. By analogy to the Edwards-Anderson model [40–42], we expect the system to exhibit a magnetic-glassy multicritical point [43–45] and develop a low-T SG phase for $x \leqslant 0.225$. We qualitatively verify this scenario by investigating both F and AF observables, as shown in Figs. 4(b)–4(d). At $x = 0.5$ the system behaves as a typical ferromagnet with a peak in the F susceptibility $\chi_F = \frac{N}{T}([\langle m^2\rangle - \langle m\rangle^2]_{dis})$ that grows with system size [Fig. 4(c)] and a saturation magnetization $\langle m^2\rangle$ that approaches unity as $T \to 0$ [Fig. 4(b)]. In contrast, at $x = 0.2$, we find competing F and AF fluctuations with broad peaks of comparable size in χ_F [Fig. 4(c)] and χ_{AF} [Fig. 4(d)], where χ_{AF} measures the susceptibility at wave vector $q = (\pi, \pi, \pi)$. Both F and AF order parameter magnetizations are small (and finite) in such a finite system [Fig. 4(b)]. We leave a detailed study of the glassy phase, and other parameter regions in this model, for future work.

We can determine the $T = 0$ boundary of the glassy phase on the lower doping side from our bond percolation analysis presented above [Fig. 3(c)], which gave $x_{SG,min} = 0.075$. Since the SG transition temperature must vanish at this point, we obtain the phase diagram shown in Fig. 4(a), which bears a striking resemblance to the experimental phase diagram in Fig. 1. Note that we focus on phase transitions below the T^* line in Fig. 1, where finite order parameters develop. This is a strong indication that our model correctly captures the microscopic physics in the low and intermediate doping range in LSCO, and that it is the frustration of polarons due to competing AF and F interactions that underlies the shift of the percolation threshold from the naively expected value $x \simeq 0.05$ to the experimentally observed value $x_c = 0.18$. Given the universality of the spin-state physics and spin-state polaron formation in other doped cobaltites, such as $La_{1-x}Ca_xCoO_3$, $La_{1-x}Ba_xCoO_3$, $Pr_{1-x}Ca_xCoO_3$, etc., and their similar qualitative behavior with doping, it is highly likely that this model can be applied far more broadly than to $La_{1-x}Sr_xCoO_3$, as corroborated by our additional simulations for larger frustration ratios (see Supplemental Material Sec. S4).

Conclusion. In essence, the model developed in this Letter reveals that a factor previously ignored in the physics of doped cobaltites—magnetic frustration—plays an inherent role in shaping their electronic/magnetic phase diagrams. Such frustration, which is of broad importance in condensed matter systems, delays the percolation associated with magnetic polarons, playing a vital role in the onset of long-range-ordered ferromagnetism in these systems. This is yet another illustration of the importance of frustration in magnetic materials. From the experimental perspective, this Letter also provides data that highlight the discrepancy between polaron percolation and the onset of ferromagnetism and offers the most definitive magnetic phase diagram to date for this material.

We provide all required programs as open-source software, and we make the raw data of our results openly accessible [46].

Acknowledgments. We acknowledge valuable discussions with B. I. Shklovskii and T. Vojta. Experimental work at the University of Minnesota (UMN) was supported by the U.S. Department of Energy through the UMN Center for Quantum Materials under DE-SC-0016371. Work at Argonne National Laboratory (crystal growth and magnetic characterization) was supported by the U.S. Department of Energy, Office of Science, Basic Energy Sciences, Materials Science and

Engineering Division. During conception and execution of the theory work, R.M.F. and P.P.O. were supported by the National Science Foundation through the UMN MRSEC under Grant No. DMR-1420013, renewed as DMR-2011401. P.P.O also acknowledges support from startup funds from Iowa State University during the late stages of the theory work.

[1] M. Imada, A. Fujimori, and Y. Tokura, Rev. Mod. Phys. **70**, 1039 (1998).
[2] S. Das Sarma, M. P. Lilly, E. H. Hwang, L. N. Pfeiffer, K. W. West, and J. L. Reno, Phys. Rev. Lett. **94**, 136401 (2005).
[3] Y. Meir, Phys. Rev. Lett. **83**, 3506 (1999).
[4] L. Zhang, C. Israel, A. Biswas, R. L. Greene, and A. de Lozanne, Science **298**, 805 (2002).
[5] T. Z. Ward, J. D. Budai, Z. Gai, J. Z. Tischler, L. Yin, and J. Shen, Nat. Phys. **5**, 885 (2009).
[6] E. Dagotto, Science **309**, 257 (2005).
[7] Y. Tokura, Phys. Today **56** (7), 50 (2003).
[8] M. A. Señarís-Rodríguez and J. B. Goodenough, J. Solid State Chem. **118**, 323 (1995).
[9] J. Wu and C. Leighton, Phys. Rev. B **67**, 174408 (2003).
[10] C. He, S. El-Khatib, J. Wu, J. W. Lynn, H. Zheng, J. F. Mitchell, and C. Leighton, Europhys. Lett. **87**, 27006 (2009).
[11] J. Wu, J. W. Lynn, C. J. Glinka, J. Burley, H. Zheng, J. F. Mitchell, and C. Leighton, Phys. Rev. Lett. **94**, 037201 (2005).
[12] D. Phelan, D. Louca, S. Rosenkranz, S.-H. Lee, Y. Qiu, P. J. Chupas, R. Osborn, H. Zheng, J. F. Mitchell, J. R. D. Copley, J. L. Sarrao, and Y. Moritomo, Phys. Rev. Lett. **96**, 027201 (2006).
[13] See Supplemental Material at http://link.aps.org/supplemental/10.1103/PhysRevMaterials.6.L071402 for details on the construction of the phase diagram in Fig. 1 (Sec. S1), on the doping evolution of the low-temperature specific heat (Sec. S2), on the results of the F Binder cumulant in the theoretical model (Sec. S3), and on simulation results for larger frustration ratios J_{33}/J_{44} (Sec. S4) and without frustration (Sec. S5).
[14] A. Podlesnyak, S. Streule, J. Mesot, M. Medarde, E. Pomjakushina, K. Conder, A. Tanaka, M. W. Haverkort, and D. I. Khomskii, Phys. Rev. Lett. **97**, 247208 (2006).
[15] M. W. Haverkort, Z. Hu, J. C. Cezar, T. Burnus, H. Hartmann, M. Reuther, C. Zobel, T. Lorenz, A. Tanaka, N. B. Brookes, H. H. Hsieh, H.-J. Lin, C. T. Chen, and L. H. Tjeng, Phys. Rev. Lett. **97**, 176405 (2006).
[16] M. A. Korotin, S. Y. Ezhov, I. V. Solovyev, V. I. Anisimov, D. I. Khomskii, and G. A. Sawatzky, Phys. Rev. B **54**, 5309 (1996).
[17] S. Noguchi, S. Kawamata, K. Okuda, H. Nojiri, and M. Motokawa, Phys. Rev. B **66**, 094404 (2002).
[18] P. M. Raccah and J. B. Goodenough, Phys. Rev. **155**, 932 (1967).
[19] G. H. Jonker and J. H. Van Santen, Physica **19**, 120 (1953).
[20] G. H. Jonker, J. Appl. Phys. **37**, 1424 (1966).
[21] A. Podlesnyak, G. Ehlers, M. Frontzek, A. S. Sefat, A. Furrer, T. Strässle, E. Pomjakushina, K. Conder, F. Demmel, and D. I. Khomskii, Phys. Rev. B **83**, 134430 (2011).
[22] C. He, S. Eisenberg, C. Jan, H. Zheng, J. F. Mitchell, and C. Leighton, Phys. Rev. B **80**, 214411 (2009).
[23] C. He, Magneto-electronic phase separation in doped cobaltites, Ph.D. thesis, University of Minnesota, 2009.
[24] R. X. Smith, M. J. R. Hoch, P. L. Kuhns, W. G. Moulton, A. P. Reyes, G. S. Boebinger, J. Mitchell, and C. Leighton, Phys. Rev. B **78**, 092201 (2008).
[25] R. X. Smith, M. J. R. Hoch, W. G. Moulton, P. L. Kuhns, A. P. Reyes, G. S. Boebinger, H. Zheng, and J. F. Mitchell, Phys. Rev. B **86**, 054428 (2012).
[26] C. He, M. A. Torija, J. Wu, J. W. Lynn, H. Zheng, J. F. Mitchell, and C. Leighton, Phys. Rev. B **76**, 014401 (2007).
[27] S. Yamaguchi, Y. Okimoto, H. Taniguchi, and Y. Tokura, Phys. Rev. B **53**, R2926 (1996).
[28] A. Podlesnyak, M. Russina, A. Furrer, A. Alfonsov, E. Vavilova, V. Kataev, B. Büchner, T. Strässle, E. Pomjakushina, K. Conder, and D. I. Khomskii, Phys. Rev. Lett. **101**, 247603 (2008).
[29] A. Alfonsov, E. Vavilova, V. Kataev, B. Büchner, A. Podlesnyak, M. Russina, A. Furrer, T. Strässle, E. Pomjakushina, K. Conder, and D. I. Khomskii, J. Phys.: Conf. Ser. **150**, 042003 (2009).
[30] D. Phelan, D. Louca, K. Kamazawa, S.-H. Lee, S. N. Ancona, S. Rosenkranz, Y. Motome, M. F. Hundley, J. F. Mitchell, and Y. Moritomo, Phys. Rev. Lett. **97**, 235501 (2006).
[31] V. G. Sathe, A. V. Pimpale, V. Siruguri, and S. K. Paranjpe, J. Phys.: Condens. Matter **8**, 3889 (1996).
[32] P. P. Orth, R. M. Fernandes, J. Walter, C. Leighton, and B. I. Shklovskii, Phys. Rev. Lett. **118**, 106801 (2017).
[33] J. Walter, T. Charlton, H. Ambaye, M. R. Fitzsimmons, P. P. Orth, R. M. Fernandes, and C. Leighton, Phys. Rev. Materials **2**, 111406(R) (2018).
[34] D. Stauffer and A. Aharony, *Introduction to Percolation Theory*, 2nd ed. (Taylor & Francis, London, 1994).
[35] B. I. Shklovskii and A. L. Efros, *Electronic Properties of Doped Semiconductors*, Springer Series in Solid-State Sciences Vol. 45 (Springer, Heidelberg, 1984).
[36] R. G. Miller, Biometrika **61**, 1 (1974).
[37] P. Tong, J. Yu, Q. Huang, K. Yamada, and D. Louca, Phys. Rev. Lett. **106**, 156407 (2011).
[38] K. Binder, Z. Phys. B **43**, 119 (1981).
[39] A. W. Sandvik, in *Lectures on the Physics of Strongly Correlated Systems XIV: Fourteenth Training Course in the Physics of Strongly Correlated Systems*, edited by A. Avella and F. Mancini, AIP Conf. Proc. Vol. 1297 (AIP, Melville, NY, 2010), p. 135.
[40] S. F. Edwards and P. W. Anderson, J. Phys. F: Met. Phys. **5**, 965 (1975).
[41] H. G. Katzgraber, M. Körner, and A. P. Young, Phys. Rev. B **73**, 224432 (2006).
[42] N. Kawashima and H. Rieger, in *Frustrated Spin Systems* (World Scientific, Singapore, 2005), pp. 491–596.
[43] P. Le Doussal and A. B. Harris, Phys. Rev. Lett. **61**, 625 (1988).
[44] M. Hasenbusch, F. P. Toldin, A. Pelissetto, and E. Vicari, Phys. Rev. B **76**, 094402 (2007).
[45] M. Hasenbusch, A. Pelissetto, and E. Vicari, Phys. Rev. B **78**, 214205 (2008).
[46] P. P. Orth, "Orth-Research/mcdis-pt: Initial release version 1.0.0 (v1.0.0)", Zenodo, doi: 10.5281/zenodo.6750991 (2022).